Published in final edited form as:
IEEE Trans Med Imaging. 2011 February ; 30(2): 224–230. doi:10.1109/TMI.2010.2072934.

Volumetric *in vivo* imaging of microvascular perfusion within the intact cochlea in mice using ultra-high sensitive optical microangiography

Hrebesh M. Subhash and **Viviana Davila**
Biophotonics and imaging lab, Division of Biomedical Engineering, School of Medicine, Oregon Health & Science University, Portland, OR 97239 USA (mollysub@bme.ogi.edu; bhatia@ohsu.edu).

Hai Sun
Department of Neurological Surgery, Oregon Health & Science University, Portland, OR 97239 USA (sunh@ohsu.edu).

Anh T. Nguyen-Huynh
Department of Otolaryngology-Head and Neck Surgery, Oregon Health & Science University, Portland, OR 97239 USA (nguyanh@ohsu.edu).

Xiaorui Shi and **Alfred L. Nuttall[Senior Member]**
IEEE, Oregon Hearing Research Center, School of Medicine, Oregon Health & Science University, Portland, OR97239 USA (nuttall@ohsu.edu).

Ruikang K. Wang
Biophotonics and imaging lab, Division of Biomedical Engineering, Oregon Health & Science University, Portland,OR97239USA

Abstract

Studying the inner ear microvascular dynamics is extremely important to understand the cochlear function and to further advance the diagnosis, prevention and treatment of many otologic disorders. However, there is currently no effective imaging tool available that is able to access the blood flow within the intact cochlea. In this paper, we report the use of an ultrahigh sensitive optical micro angiography (UHS-OMAG) imaging system to image 3D microvascular perfusion within the intact cochlea in living mice. The UHS-OMAG image system used in this study is based on spectral domain optical coherence tomography, which uses a broadband light source centered at 1300nm with an imaging rate of 47,000 A-scans per second, capable of acquiring high-resolution *B* scans at 300 frames/sec. The technique is sensitive enough to image very slow blood flow velocities, such as those found in capillary networks. The 3D imaging acquisition time for a whole cochlea is ~4.1 sec. We demonstrate that volumetric reconstruction of microvascular flow obtained by UHS-OMAG provides a comprehensive perfusion map of several regions of the cochlea, including the otic capsule, the stria vascularis of the apical and middle turns and the radiating arterioles that emanate from the modiolus.

Keywords

Biomedical optical imaging; Blood flow measurement; optical interferometry; optical coherence tomography; optical microangiography

R.K. Wang (Corresponding author) (wangr@ohsu.edu)..

I. Introduction

Detailed knowledge of cochlear vascular anatomy and perfusion are essential for understanding the function of hearing and the pathophysiology of several otologic disorders, such as, noise induced hearing loss, endolymphatic hydrops and presbycusis, which are thought to involve an abnormal regulation of cochlear blood flow (CoBF) [1]-[3]. Moreover, normal blood supply to the cochlea is critical to generating the ionic concentrations required for auditory transduction, the mechanism by which sound waves are converted to nerve impulses that are carried by the 8th nerve and auditory pathway to the cortex [4]-[5]. The cochlear lateral wall receives its blood supply from a tight network of extremely slender vessels emanating from the central core of the cochlea (modiolus). Further understanding of the relation between the dynamics of cochlear blood flow and hearing function is important for improving diagnosis and treatment of sensorineural hearing loss that potentially arises from circulatory abnormalities. However, it has been difficult to find direct evidence of CoBF impairment in various kinds of sensorineural hearing loss in humans. This is largely because there is currently no effective imaging tool available to directly observe the blood flow and vasculature within the cochlea that is surrounded by bone (otic capsule). A non-invasive and depth-resolved imaging tool that can measure the CoBF of micron-scale vessels within the intact inner ear *in vivo* would represent a major advance in cochlear microcirculation research and for clinical practice.

Although a number of *in vivo* imaging modalities have been developed to visualize the micro-circulation of the human inner ear, the main limitation of most of these studies is that they provide relative changes in blood flow rather than absolute flow rates within individual vessels. One of the imaging modalities currently used to visualize inner ear perfusion is dynamic contrast enhancement magnetic resonance imaging (MRI) [6]. MRI has sufficient spatial resolution to visualize the macro-anatomy of the cochlea [7]-[8]. However, even with the highest spatial resolution technique, MRI cannot resolve the microvascular network within the inner ear [9]. On the other hand, Doppler ultrasonographic methods have revealed several blood flow disturbances related to inner ear diseases, such as Meniere's disease [10] and idiopathic sudden sensorineural hearing loss [11]. However, the spatial resolution of Doppler ultrasonography is still limited when evaluating intra-cochlear anatomical structures because it has a shallow penetration depth when imaging through bone, such as the otic capsule that surrounds the cochlea located deep within the skull. Moreover, the acoustic trauma induced by the high acoustic frequencies used in Doppler ultrasonography is a major concern, since it may cause damage to the hearing mechanism. Laser-Doppler flowmetry is another modality that is widely used for the evaluation of cochlear blood flow. This method relies on the Doppler effect of photons that are reflected when a laser beam is directed at the tissue under study [12]. The laser Doppler approach is able to measure cochlear blood flow, but only in those animal species whose otic capsule is relatively thin, so attenuation of the incident and reflected laser beams is weak [13]-[14]. Despite the ability of the laser Doppler method to measure CoBF, it cannot spatially resolve the dense capillary network within the stria vascularis, a vascular structure of the lateral wall where homeostatic regulation of CoBF is critical for hearing. Although several intravital microscopy studies of cochlear blood flow in laboratory animals have enabled visualization of blood flow within individual vessels [15]-[19], they typically involved extensive surgical resection of the temporal bone, which may damage the delicate structure and microvascular network in the inner ear; moreover, they achieve only shallow penetration depths and a limited field of view.

As a variation of optical coherence tomography technology [20]-[21], Optical microangiography (OMAG) [22] is a recently developed imaging modality that is capable of imaging slow microcirculation down to micro capillary level resolution, within tissue beds up to 2.00 mm beneath the tissue surface. The imaging contrast of blood perfusion in

OMAG is based on endogenous light scattering from moving blood cells; thus, no exogenous contrast agents are necessary for imaging. In OMAG imaging, in order to separate the moving scatters from static one, a constant modulation frequency was introduced into the spectral interferogram along the B-scan direction. This modulation frequency can be introduced either by using a moving reference arm mirror mounted onto a linear piezo-translational stage or by offsetting the scanning probe beam on the x-scanning mirror in the sample. The feasibility of OMAG for imaging cerebral blood flow in mice [23]-[24] and ocular blood flow in human has been successfully demonstrated [25]. Most recently, we have shown the potential of OMAG in imaging CoBF within the intact cochlea in gerbil in vivo [26]. In this reported OMAG system, the modulation frequency was introduced by moving the reference arm mirror at 300μm/s, which was mounted onto a linear pizo-translational stage. Only blood cells moving at a rate higher than 300 μm/s toward the surface will get mapped into the blood perfusion image. Thus the minimal blood flow imaging of the system was 300 μm/s – a limit empirically determined by the modulation frequency of the reference arm and as well as the optical heterogeneous properties of the cochlea tissue. However, Nuttall [27,28] indicated that the velocity of flow in the lateral wall capillaries ranges from 30 to 140 μm/s. Thus, the previous study that employed OMAG only visualizes the faster CoBF in blood vessels, most likely in arterioles and venules. To observe the flow dynamics in the capillary beds within the lateral walls in the cochlea, the sensitivity of OMAG to the blood flow must be improved.

In this paper, we propose the use of an ultrahigh sensitive OMAG (UHS-OMAG) to image the capillary CoBF in the intact cochlea. We first describe the UHS-OMAG system setup, and then introduce a novel scanning protocol and image processing algorithm into OMAG imaging method to improve OMAG imaging sensitivity to the slow capillary flows within the intact cochlea in mice. Finally, we demonstrate the feasibility of UHS-OMAG to obtain a depth resolved 3D microvascular perfusion map of CoBF in live mouse. To the best of our knowledge, this is the first demonstration of 3D *in vivo* microvascular imaging of cochlear capillaries in a live rodent.

II. MATERIALS AND METHODS

A. System setup

The schematic of the experimental setup is shown in Fig.1. Briefly, light from a 56 nm bandwidth low-coherence broadband infrared superluminescent diode light source (1300±28 nm) is split into two paths in a 10:90 fiber based Michelson interferometer. One beam is coupled onto a stationary reference mirror and the second was focused and scanned using a pair of galvo mirrors. The light emerging at the output of the interferometer was sent to a custom-built high-speed spectrometer. The spectrometer consists of a transmission grating (1175 lines/mm), a camera lens with a focal length of 100 mm, and a 1024 element line scan infrared InGaAs detector with a 25 μm pixel pitch size. The spectral resolution of the designed spectrometer was around 0.141 mm, which provided a total depth range of ~3.0 mm in air (2.22mm in biological tissue by assuming the refractive index of the sample is ~1.35). The axial resolution of the system was 13 μm in air (~9.6 μm in tissue). We used an objective lens with a focal length of 50 mm to deliver the probe beam onto the sample, providing a transverse resolution of ~16μm and a depth of focus of ~2 mm.

B. Scanning protocol and image reconstruction algorithm

Unlike conventional OMAG, to achieve ultrahigh sensitive imaging of slow microcirculation, UHS-OMAG employs a new scanning protocol and novel flow reconstruction algorithm. UHS-OMAG acquires low density B-scan frame (i.e. x-direction scan) with 128 A-lines with a spacing of ~11.5μm (which is of the order of the least

sampling distance of 10 μm for the system lateral resolution of 16 μm) between adjacent A-lines, which covers a total x-scan range of ~1.5mm. In our system, the integrating time was set at 17 μs and the maximum line rate of the camera was 47 KHz, which corresponds to a theoretical imaging rate of 367 frames per second (fps). However, by using CameraLink ™ and a high-speed frame grabber board (PCI 1428, National Instruments, USA), the maximum achievable frame rate was 300 fps, limited by the hand shake time between the camera and the host computer. We employed a high density C-scan (i.e. in Y-direction), which encompasses 1250 B-scan over a range of 1.25mm along the Y-direction with an over sampling factor of ~20. The spacing between adjacent B-scans was ~1 μm. The system requires only ~4.1 seconds to capture a 3D volume data set of a whole cochlea.

The C-scan spectral interference signals captured by the UHS-OMAG system can be written as:

$$I\left(t,k_j\right)=S\left(t,k_j\right)\left\{E_R^2+2E_R\int_{-\infty}^{\infty}a\left(z,t\right)\cos\left[2k_jn\left(t\right)z\right]dz+2E_Ra\left(z_l\right)\cos\left[2k_jn\left(t\right)\left(z_l-vt\right)\right]\right\} \quad (1)$$

where $j=1,2,\ldots,1024$ is the pixel number of the line scan CCD camera, k_j is the wave number of the light captured by the j^{th} pixel; $I(k_j)$ is the light intensity detected by the j^{th} detector; t is the time variable when one A-line, $I(k)$, was captured in the Y-direction (C scan direction), as show in Fig.2; $S(k_j)$ is the spectral density of the light source at k_j; n is the refractive index; $a(z)$ is the amplitude of the back scattered light and z is the depth from which the light back scattered from; v is the velocity of a moving particle, for example blood cells, which are buried in the tissue at depth z_1. In Eq. (1), we ignore the self cross-correlation term that occurred between the light backscattered within the sample, because it is relatively weak compared to that reflected from the reference mirror. Then the first term in Eq. (1) is the DC signal produced by the light reflected from the reference mirror. The second term is the spatial frequency component of the static tissue sample, which we call the heterogeneous frequency component, which can provide the static structural information of the sample. The third term is the Doppler beating signal, which is introduced by the moving particles in the tissue sample. Depending upon the magnitude of the moving particles velocity, the Doppler beating signal shifts away from the static interference signals caused by the microstructures of the sample. .

For obtaining slow the microcirculation within capillary vessels, UHS-OMAG algorithm uses the high pass filtering along the C-scan direction as shown in Fig.2, rather than in the B-scan direction in conventional OMAG, in order to remove the DC signal and the static signals due to the microstructures of the sample. In UHS-OMAG thus, the maximum detectable velocity that is not wrapped is determined by the adjacent time spacing, Δt_B, between adjacent B-scans in the Y-direction, i.e., $V=\lambda/2n\Delta t_B$, where λ is the central wave length of the light source. In our system imaging system, the B-scan frame rate is 300fps, i.e., Δt_B~3.3ms. Therefore, considering that the C-scan direction is densely sampled with an oversampling factor of ~20, the maximum unambiguous detectable velocity would be 141μm/s. It must be emphasized that the maximum velocity that can be detected by the system is determined by the system imaging speed. Here, the imaging speed is of an A-scan rate of 47,000 per second. Under this circumstance, the maximum detectable velocity is ~30 mm/s. However, if flow velocity is >141μm/s, the UHS-OMAG will not be able to provide the actual velocity values because of the well-known phase wrapping effect in the interference signals, unless a specific phase-unwrapping algorithm is used to un-wrap the phases.

The minimum velocity that the system can detect is determined by the system phase noise floor, which can be expressed by the intensity signal to noise ratio, S, of the OMAG/OCT system by $\sigma_{\Delta\varphi}^2=1/S$ [27,28]. At an imaging speed of 47,000 A-scan per second, we

measured the system signal to noise ratio to be 85 dB. In order to estimate the minimum detectable velocity, we experimentally measured the phase noise of our UHS-OMAG system with a flow phantom as the imaging target. The phantom was made of gelatin mixed with ~1% of milk to simulate the back ground optical heterogeneity of the tissue. A capillary tube with an inner diameter of ~400μm was submerged in the gel and a ~2% TiO_2 particle solutions was flowing into it using a precision syringe pump. To qualitatively analyzing the minimum resolvable velocity, we applied the phase-resolved technique [23] into the adjacent B-scans of the UHS-OMAG flow images to provide the velocity map of the flow phantom. Thus, the observed minimal detectable flow velocity was ~4.0 μm/s.

Therefore, the detectable blood flow of the UHS-OMAG system would range from ~4 μm/s to ~30 mm/s, which is sufficient to image the CoBF in rodent microcapillaries.

The high pass filtering in our proposed signal processing is implemented by applying a differential operation on the captured B-scan spectral interferograms along the C-scan direction. The differential operation is equivalent to high pass filtering, which suppresses the DC and scattering signals from the static elements within the scanned volume, i. e.,

$$I_{FLOW}\left(t_i, k_j\right) = I\left(t_i, k_j\right) - I\left(t_{i-1}, k_j\right), i = 1, 2, 3 \ldots\ldots 1250 \quad (2)$$

where i represents the index of the B-scans in the C-scan direction. Then, by applying the fast Fourier transform (FFT) upon every wavenumber k (keeping t constant) the depth resolved blood flow signals are obtained, where λ-k is obtained by using cubic spline interpolation on the captured interferogram. The movement artifact is one of the most distracting issues for *in vivo* imaging of slow microcirculations, which is caused by the involuntary movement of sample and can seriously deteriorate the image quality. In our previous work [23], we proposed a phase compensation method to effectively resolve this issue in the traditional OMAG system. In our UHS-MAG system, we directly implemented this phase compensation method to minimize the movement artifact issues.

C. Animal model and surgical technique

Healthy C57 BL/6 mice weighing around 20 to 30 gm (3 month old) were used in this study. The experimental protocol was in compliance with the Federal guidelines for care and handling of small rodents and approved by the Institutional Animal Care and Use Committee (IACUC) of Oregon Health and Science University (OHSU).

Animals were initially anesthetized by a single intra-peritoneal (i.p.) injection of ketamine (75mg/kg) and xylazine (10mg/kg). The mouse was then placed on a heating pad and maintained at 37 ±1°C. Prior to surgically exposing the cochlea, the mouse was immobilized and positioned onto an imaging platform to minimize movements, which is essential for *in vivo* imaging.

Using sterile surgical techniques, a ventral approach through the neck was used to access the tympanic bulla [29]. This approach provides access to the inner ear with minimal blood loss or mortality and allows for a direct view of the lateral wall vessels within the middle and basal cochlear turns and of the round window niche area. After incision, the left submandibular gland and posterior belly of digastric muscle were removed by cauterization and a well-defined sternocleidomastoid muscle and facial nerve extending anteriorly toward the bulla were identified. The bony bulla was exposed and the dorsal region of the bulla was surgically removed, providing a clear view of the cochlea and the stapedial artery (SA), with its medial margin laying over the edge of the round window niche, coursing anterior-superiorly towards the oval window.. Fig.3A shows the ventral view of the surgical site. Fig. 3B shows a close up view of the rectangular region (black) in Fig.3A. The middle turn,

arrow, and basal turn, arrowhead, of the cochlea are seen. The apical turn of the cochlea is buried in the shadows at the top of the image and not visible. The head of the malleus and a portion of the stapedial artery are also visible and labeled. After surgery, the anesthetized mouse with exposed intact cochlea (Fig. 3) was moved under the UHS-OMAG imaging probe. The side of the exposed cochlea was aimed toward the probe beam in order to obtain a clear view of the lateral wall vessels located just beneath the intact otic capsule surrounding the cochlea. During imaging, an additional general anesthesia with isoflurane (0.2 L/min O_2, 0.8 L/min air) was applied and the breathing interval of the animal was controlled by adjusting the concentration of isoflurane in the vaporizing chamber of the anesthetic station.

III. Results

In vivo visualization of microvascular perfusion in the intact mouse cochlea was obtained through a wide opening through the bulla using UHS-OMAG. Obviously, the in-vivo condition is required for the images, because it is the motion due to flow that is detected and forms the image. The axis of the cochlea through the modiolus was oriented at an 80° angle relative to the imaging beam, such that a small portion of the apical turn and helicotrema as well as the middle turn of the cochlea are visible at the beginning of the lateral B-scan 2D cross-sectional flythrough (Fig 5B). Moreover, this alignment provide enough Doppler angle (80°) to obtain Doppler-induced signals from any horizontally oriented vascular network in the imaging region. As the C-scan progresses in the medial direction (y-direction) across the cochlea, two sections of the middle turn meet, where a cross-section of Reissner's membrane appears like a single line that approaches the far lateral wall of the cochlea. Fig.4A (Media1) shows a 3D volumetric projection image of the cochlear microanatomy obtained by UHS-OMAG . The dashed line in Fig 4A indicates the first B Scan. To reveal the internal cochlear turns more clearly, the image transparency was increased with the 3D reconstruction software. Fig.4B illustrates how the turns of the cochlea are designated, (apical turn, *A*, middle turn, *M* and basal turn, *B*), the location of the stapedial artery (SA), what portion of the cochlea is imaged (dashed lines) and C scan direction (arrow). In Fig. 4A, the end of apical turn and helicotrema as well as parts of the middle and basal turns that are directly opposed the imaging beam are clearly seen. The regions of the cochlea that are either located deep within the tissue or under thick bone toward the edge of the bulla could not be imaged with our UHS-OMAG imaging system.

Fig.5A shows an *en-face* (x-y) projection view of the perfusion through the vascular network located in the upper surface of the cochlea imaged with UHS-OMAG, (compare the location of the stapedial artery and C scan direction in Fig. 4B as a reference). The obtained results clearly provide the visualization of depth resolved microvascular map of cochlea without quantitative flow information. Radiating arterioles feeding the stria vascularis (SV) emanate from the modiolus (M) and traverse over the scala vestibuli of the middle turn, *arrowheads*. The stria vascularis of the apical, middle and middle basal turn (SVm) are seen very clearly, but the radiating arterioles that feed the basal turns are obscured by the middle turn. The collecting venules that run over the scala tympani of both turns are not visible in this image.

Fig.5B shows the first B scan microvascular perfusion image of a cross-section through the middle and apical turns of the cochlea corresponding to the line drawn in Fig.5A. The imaging beam is directed down onto the surface of the cochlea (top of the image) and the major structures of the middle turn are labeled. Reissner's membrane (RM) and the basilar membrane (BM) can be detected with UHS-OMAG, as well as perfusion through the vessels of the otic capsule and the lateral wall, a thin layer of membrane lining the inside of the bony otic capsule that faces the sensory transduction cells. A portion of the blood flow

through the lateral wall between Reissner's membrane and the basilar membrane appears denser and spatially corresponds to the dense capillary bed of the stria vascularis of the middle turn (SV). The vasculature of the bony otic capsule is less dense than in the lateral wall and, therefore, the pixel intensity is also lower, which indicates less blood flow. The full fly-through B-scan scan along the C-scan direction (Y-axis) is provided in Supplementary Information (Media2).

In order to demonstrate the feasibility of UHS-OMAG to resolve slow velocities, we scanned the 2-D cross-sectional image of capillary beds of the stria vascularis of the middle turn at fixed plane. Fig.6 (A) and (B) shows the 2D cross-sectional image of the flow map obtained by UHS-OMAG and the velocity map, respectively. The velocity map is obtained by calculating the phase differences between adjacent B-scans. The white arrows pointing bright spots in the velocity map are corresponding to capillaries with blood flow in the forward direction.

Fig.7 A (Media3) and B (Media4) show two 3D volumetric reconstructions of the microvascular perfusion in the cochlea that are rendered in two different orientations. The 3D volumetric image clearly reveals that the arterial blood supply to the lateral wall is emanating from the modiolus, which also contains the cochlear nerve (not visible in these images). Fig.7 C (Media5) shows the segmented 3D volumetric image of the arteries emanating from the modiolus. A 3D volumetric image of the combined microvascular perfusion and structural data is shown in Fig.6D (Media6). In normal rodents, such as in guinea pig, rat or mouse, the optical observation of blood flow using intravital microscopy indicates that the velocity among different cochlear microvascular structures, including the stria vascularis, ranges from 30μm/s to 140 μm/s [17]. The sensitivity of UHS-OMAG is high enough to obtain depth resolved microvasculature images of slow perfusion flow rates, as would be expected in the capillaries of the stria vascularis. The results presented in this study clearly show the potential of UHS-OMAG to access inner ear microcirculations and should provide improved diagnostic capability and therapeutic intervention in both clinical and fundamental research.

IV. Conclusion

The study of the relationship between cochlear blood flow and hearing has been limited by the inaccessibility of the microvasculature for non-invasive observation, because measurements could not be made without removing a portion of the bone surrounding the cochlea, which disturbs the delicate homeostatic balance of the cochlea. In this article, we have demonstrated that the microvascular perfusion within intact cochlea in mice can be visualized by the UHS-OMAG imaging modality. The sensitivity of UHS-OMAG is high enough to obtain depth resolved microvascular images in several regions of the cochlea, including the otic capsule, the lateral wall, (including the stria vascularis) of the apical and middle turns, and the arterioles that emanate over the apical and middle turns from the modiolus. We have shown that the current system is capable of obtaining 3D volumetric data with a temporal resolution of ~4sec. However, the lateral resolution (~20 μm) of the current system is still not high enough to resolve individual capillaries in the lateral wall within the cochlea. In the future, we plan to improve upon the UHS-OMAG imaging system with a high numerical aperture (NA) microscopic objective that may provide sufficient resolution power to resolve individual capillaries of the stria vascularis and the flow within this important structure.

In clinical point of view, the further development of the system based on surgical probes such as the endoscope and laryngoscope, which might be very useful for inner ear

intervention in both human subjects and animals through the round window even though the accessibility is limited .

Supplementary Material

Refer to Web version on PubMed Central for supplementary material.

Acknowledgments

The authors thank Mr. Lin An for assisting in optical system developments, and Drs. Wenxuan He and Tianying Ren for surgical training in the ventral approach to access the cochlea in mouse. The content is solely the responsibility of the authors and does not necessarily represent the official views of grant giving bodies.

This work was supported in part by the National Institute of Deafness and Other Communication Disorders under Grants R01DC010201, R01DC010399, R01 DC000105, and R03DC008888 and also partially supported by award number KL2RR024141 from the National Center for Research Resources.

References

1. Le Prell CG, Yamashita D, Minami SB, Yamasoba T, Miller JM. Mechanisms of noise-induced hearing loss indicate multiple methods of prevention. Hear. Res. 2006; 226:22–43. [PubMed: 17141991]
2. Seidman MD, Quirk WS, Shirwany NA. Mechanisms of alterations in the microcirculation of the cochlea. Ann. NY Acad. Sci. 1999; 884:226–232. [PubMed: 10842596]
3. Miller JM, Ren TY, Nuttall AL. Studies of inner ear blood flow in animals and human beings. Otolaryngol. Head Neck Surg. 1995; 112:101–113. [PubMed: 7816443]
4. Nakashima T, Naganawa S, Sone M, Tominaga M, Hayashi H, Yamamoto H, Liu X, Nuttall AL. Disorders of cochlear blood flow. Brain Res. 2003; 43:17–28.
5. Wangemann P. Cochlear blood flow regulation. Adv. Otorhinolaryngol. 2002; 59:51–57. [PubMed: 11885661]
6. Yamasoba T, Kikuchi S, Higo R, O'Uchi T, Tokumaru A. Sudden sensorineural hearing loss associated with slow blood flow. Ann. Otol. Rhinol. Laryngol. 1993; 102:873–7. [PubMed: 8239350]
7. Szirmai A, Kustel M, Panczel G, Kocher I, Repassy G, Nagy Z. Evidences of vascular origin of cochleovestibular dysfunction. Acta Neurol. Scand. 2001; 104:68–71. [PubMed: 11493220]
8. Shinohara S, Yamamoto E, Saiwai S, Tsuji J, Muneta Y, Tanabe M, Sakamoto T, Kim T. Clinical features of sudden hearing loss associated with a high signal in the labyrinth on unenhanced T1-weighted magnetic resonance imaging. Eur. Arch. Otorhinolaryngol. 2000; 257:480–484. [PubMed: 11131373]
9. Naganawa S, Ito T, Iwayama E, Fukatsu H, Ishigaki T, Nakashima T, Ichinose N. MR Imaging of the labyrinth: Current capabilities and future challenges. Radiology. 1999; 213(P):547.
10. Gortan D. Transcranial Doppler sonography in patients with Meniere's disease. Acta Med. Croat. 2000; 54:11–14.
11. De Felice C, De Capua B, Tassi R, et al. Non-functioning posterior communicating arteries of circle of Willis in iiopathic sudden hearing loss. Lancet. 2000; 356:1237–8. [PubMed: 11072945]
12. Shepherd, AP.; Oberg, PA. Laser-Doppler blood flowmetry. In: Borgos, J., editor. Kluwer Academic Publishers. TSI's LDV blood flowmeter; Boston: 1990. p. 73-92.
13. Nakashima T, Suzuki T, Iwagaki T, Hibi T. Effects of anterior inferior cerebellar artery occlusion on cochlear blood flow—a comparison between laser-Doppler and microsphere methods. Hear. Res. 2001; 162:85–90. [PubMed: 11707355]
14. Mom T, Telischi FF, Lonsbury - Martin BL, Martin GK. Measuring cochlear blood flow and distortion product-otoacoustic emissions during reversible cochlear ischemia: a rabbit model. Hear Res. 1990; 133:40–52. [PubMed: 10416863]
15. Axelsson A, Nuttall AL, Miller JM. Observations of cochlear microcirculation using intravital microscopy. Acta Otolaryngol. 1990; 109:263–70. [PubMed: 2316348]

16. Nuttall AL. Velocity of red blood cell flow in capillaries of the guinea pig cochlea. Hear Res. 1987; 27:121–8. [PubMed: 2440843]
17. Nuttall AL. Techniques for the observation and measurement of red blood cell velocity in vessels of the guinea pig cochlea. Hear Res. 1987; 27:111–9. [PubMed: 2440842]
18. Prazma J, Carrasco VN, Garrett CG. Measurement of cochlear blood flow: intravital fluorescence microscopy. Hear Res. 1989; 42:229–36. [PubMed: 2514176]
19. Ren T, Lin X, Nuttall AL. Polarized-light intravital microscopy for study of cochlear microcirculation. Microvasc Res. 1993; 46:383–93. [PubMed: 8121321]
20. Fercher AF, Drexler W, Hitzenberger CK, Lasser T. Optical Coherence Tomography – Principles and Applications. Rep. Prog. Phys.,. 2003; 66:239–303.
21. Tomlins PH, Wang RK. Theory, development and applications of optical coherence tomography. J Phys. D: Appl. Phys. 2005; 38:2519–2535.
22. Wang RK, Jacques SL, Ma ZH, Hanson S, Gruber A. Three Dimensional Optical Angiography. Opt. Express. 2007; 15:4083. [PubMed: 19532651]
23. Wang RK, An L. Doppler optical micro-angiography for volumetric imaging of vascular perfusion in vivo. Opt. Express. 2009; 17:8926–8940. [PubMed: 19466142]
24. Jia YL, Alkayed NJ, Wang RK. The Potential of Optical Micro-angiography to Monitor Cerebral Blood Perfusion and Vascular Plasticity Following Traumatic Brain Injury in Mice in vivo. Journal of Biomedical Optics,. 2009; 14:040505. [PubMed: 19725710]
25. An L, Wang RK. In vivo volumetric imaging of vascular perfusion within human retina and choroids with optical micro-angiography. Opt. Express. 2008; 16:11438–11452. [PubMed: 18648464]
26. Choudhury N, Chen F, Shi X, Nuttall AL, Wang RK. Volumetric Imaging of Blood Flow Within Cochlea in Gerbil In Vivo. IEEE Journal of Selected Topics in Quantum Electronics. 2009; PP(Issue: 99)
27. Vakoc BJ, Yun SH, de Boer JF, Tearney GJ, Bouma BE. Phase-resolved optical frequency domain imaging. Opt. Express. 2005; 13:5483–5492. [PubMed: 19498543]
28. Park BH, Pierce MC, Cense B, Yun SH, Mujat M, Tearney GJ, Bouma BE, de Boer JF. Real-time fiber-based multi-functional spectral-domain optical coherence tomography at 1.3 μm. Opt. Express. 2005; 13:3931–3944. [PubMed: 19495302]
29. Jero J, Tseng CJ, Mhatre AN, Lalwani AK. A surgical approach appropriate for targeted cochlear gene therapy in the mouse. Hear Res. 2001; 151:106–114. [PubMed: 11124456]

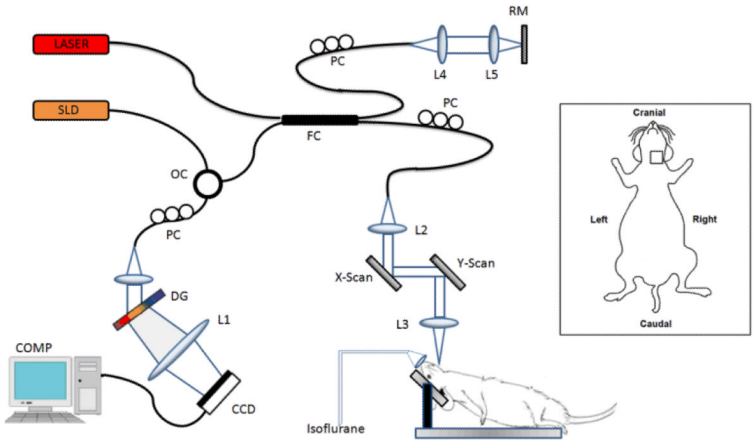

Fig.1.

Experimental setup of UHS-OMAG system: SLD – superluminescent diode, OC – optical circulator, FC– 10:90 fiber coupler, PC – polarization controller, L1-L5 – lenses, RM – reference mirror, Laser- pilot laser for beam guiding, DG – diffraction grating, CCD – line-scan camera, COMP – computer. (Inset shows the ventral view of the mouse and rectangle box shows the surgical location)

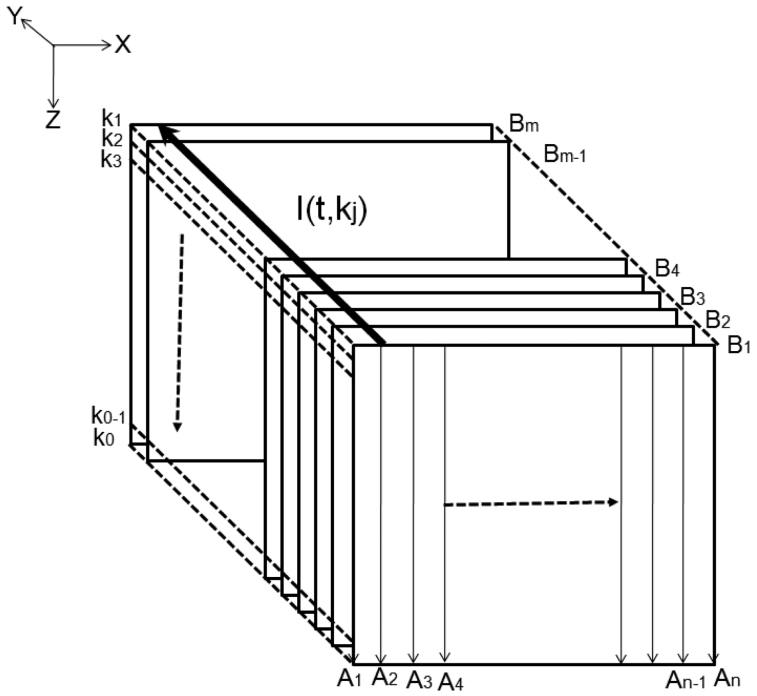

Fig.2.

Schematic of scanning protocol and signal processing method employed in UHS-OMAG. B_1 to B_m are the B-scans in the 3D data cube, where m=1250, A_1 to A_n are the A-scan in B fame where n=128. k_j is the wavenumber of the light captured by the j^{th} pixel, where where *j=1,2, …, 1024* is the pixel number of the line scan CCD camera. The solid black arrow shows the high pass filtering direction in UHS-OMAG signal processing.

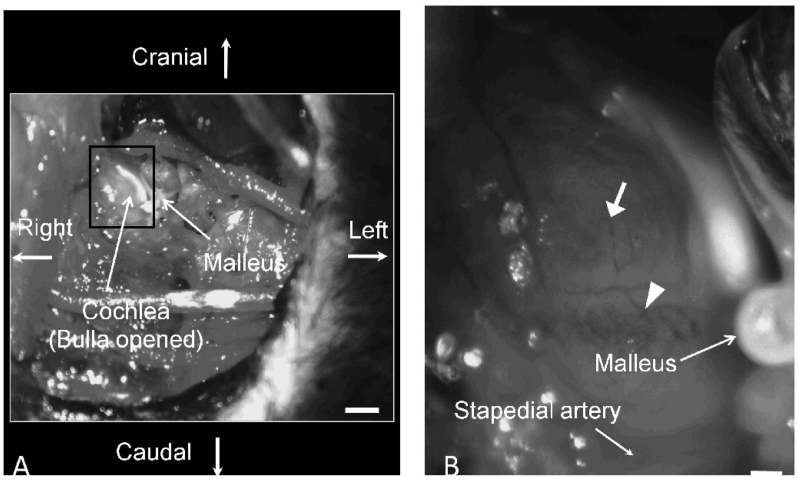

Fig.3.

Surgical view of the left cochlea in mouse. A) Ventral surgical window through the bulla exposes the middle and basal turns of the cochlea (within the rectangular box). White scale bar = 1mm; B) Optically magnified view of the exposed cochlea within the rectangular region shown in Fig. 3A.. White scale bar = 200μm.

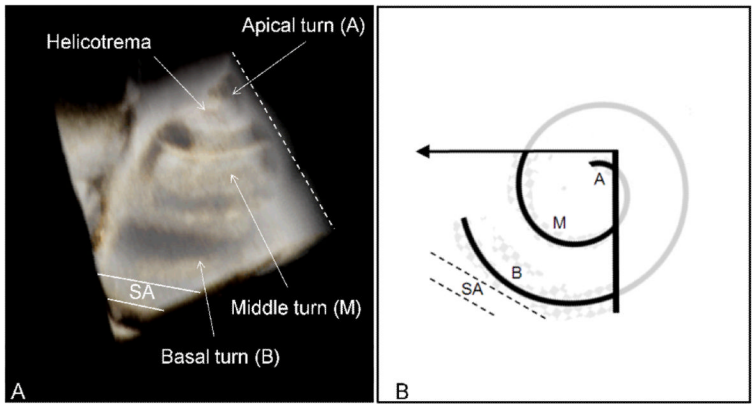

Fig.4.

A) 3D volumetric projection image of the cochlear microanatomy (**Media1**). Dashed line indicates the location of the first B scan. B) Schematic view in Fig 4A showing the imaged and non-imaged areas of the cochlea (black and grey spiral, respectively), how the turns of the cochlea are designated (apical turn - A, middle turn - M, basal turn – B), the location of the stapedial artery (SA), the first B scan (bold line) and direction of the C scan (arrow).

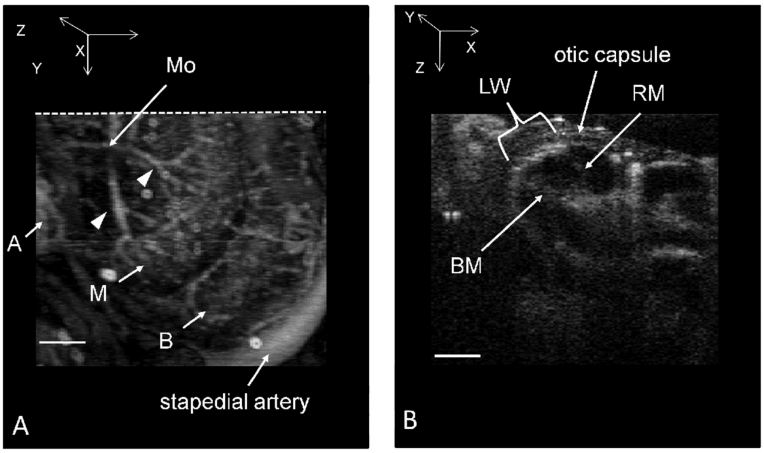

Fig.5.

A) 3D volumetric projection image of the cochlear microvascular network. The vessels imaged here are of the modiolus (Mo) and the otic capsule, lateral wall and stria vascularis of the cochlear turns that were located within the penetration depth of our imaging system. Apical vessels (A), middle turn vessels (M), and basal turn vessels (B). Radiating arterioles over the middle turn are indicated by *arrowheads*. B) Microvascular perfusion image of B-scan cross-section through the cochlea corresponding to the dotted line drawn in Fig.5A. Structures of the middle turn are labeled; Reissner's membrane (RM), basilar membrane (BM) and lateral wall, including the stria vascularis (LW). Fly through of the 2D cross-sectional images of the cochlea of the various turns can be seen in the Supplementary Information section (QuickTime, 1740 KB - **Media2**. Compare the imaging area with Fig. 4B). Scale bar = 200 μm.

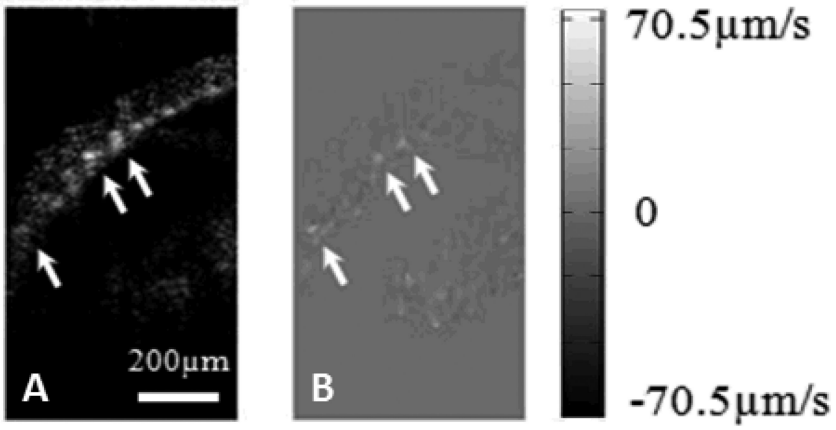

Fig.6.

A) 2D cross-sectional perfusion image of the stria vascularis of the middle turn of the cochlea. B) Velocity map obtained by taking the phase difference between adjacent B-scans.

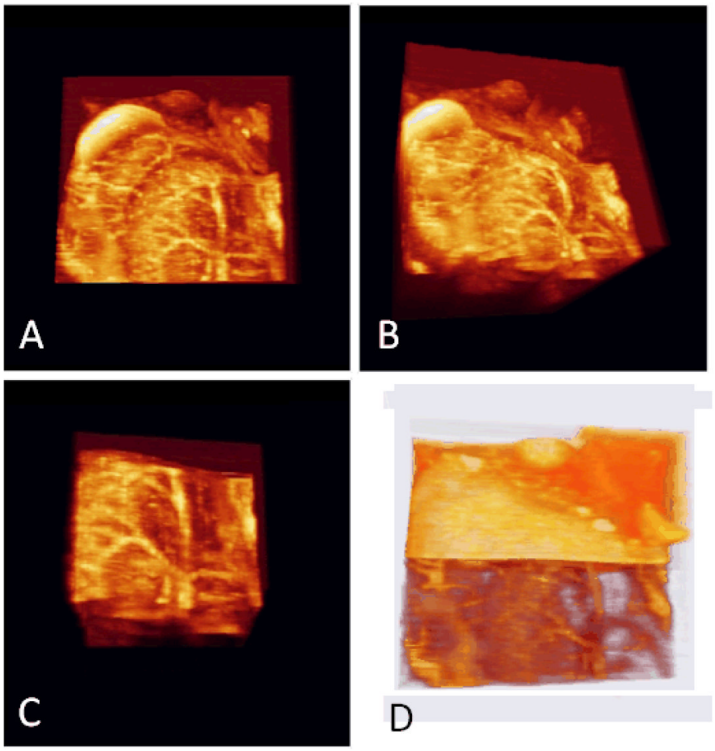

Fig.7.

3D volume rendering of microvascular anatomy of mouse cochlea, which is segmented and displayed in four different orientations to provide a detailed view of the cochlear microvascular perfusion. A&B) 3D volumetric perfusion image of the entire cochlea imaged (**Media3 & Media4**) C) Segmented 3D volumetric microvascular perfusion at the Modiolus (**Media5**). D) 3D volumetric reconstruction of microvascular perfusion together with cochlear structure (**Media6**).